HHS Public Access

Author manuscript

Biomech Model Mechanobiol. Author manuscript; available in PMC 2023 September 28.

Published in final edited form as:

Biomech Model Mechanobiol. 2018 October ; 17(5): 1533–1542. doi:10.1007/s10237-018-1039-2.

Effects of Hydrogel Injection on Borderzone Contractility Post Myocardial Infarction

Hua Wang, PhD[1,7], **Christopher B. Rodell, PhD**[2], **Xiaoyan Zhang, PhD**[1], **Neville N. Dusaj, MS**[2], **Joseph H. Gorman III, MD**[3,4], **James J. Pilla, PhD**[3,5], **Benjamin M. Jackson, MD**[4], **Jason A. Burdick, PhD**[2], **Robert C. Gorman, MD**[3,4], **Jonathan F. Wenk, PhD**[1,6,*]

[1]Department of Mechanical Engineering, University of Kentucky, Lexington, KY 40506, USA

[2]Department of Bioengineering, University of Pennsylvania, Philadelphia, PA 19104, USA

[3]Gorman Cardiovascular Research Group, Department of Surgery, University of Pennsylvania, Philadelphia, PA 19104, USA

[4]Department of Surgery, University of Pennsylvania, Philadelphia, PA 19104, USA

[5]Department of Radiology, University of Pennsylvania, Philadelphia, PA 19104, USA

[6]Department of Surgery, University of Kentucky, Lexington, KY 40506, USA.

[7]Department of Mechanical Engineering, Ludong University, Yantai, Shandong, China

Abstract

Injectable hydrogels are a potential therapy for mitigating adverse left ventricular (LV) remodeling after myocardial infarction (MI). Previous studies using magnetic resonance imaging (MRI) have shown that hydrogel treatment improves systolic strain in the borderzone (BZ) region surrounding the infarct. However, the corresponding contractile properties of the BZ myocardium are still unknown. The goal of the current study was to quantify the in vivo contractile properties of the BZ myocardium post-MI in an ovine model treated with an injectable hydrogel. Contractile properties were determined 8 weeks following posterolateral MI by minimizing the difference between in vivo strains and volume calculated from MRI and finite element model predicted strains and volume. This was accomplished by using a combination of MRI, catheterization, finite element modeling, and numerical optimization. Results show contractility in the BZ of animals treated with hydrogel injection was significantly higher than untreated controls. End-systolic (ES) fiber stress was also greatly reduced in the BZ of treated animals. The passive stiffness of the treated infarct region was found to be greater than the untreated control. Additionally, the wall thickness in the infarct and BZ regions were found to be significantly higher in the treated animals. Treatment with hydrogel injection significantly improved BZ function and reduced LV remodeling, via altered MI properties. These changes are linked to a reduction in the ES fiber stress in the BZ myocardium surrounding the infarct. The current results imply that injectable hydrogels could be a viable therapy for maintaining LV function post-MI.

*Corresponding Author: Jonathan F. Wenk, Ph.D., University of Kentucky, Department of Mechanical Engineering, 269 Ralph G. Anderson Building, Lexington, KY 40506-0503, wenk@engr.uky.edu.

Disclosures

No conflicts of interest, financial or otherwise, are declared by the author(s).

Keywords

Biomaterial; Left Ventricular Remodeling; Mechanical Properties; Magnetic Resonance Imaging; Finite Element Analysis

Introduction

Left ventricular (LV) remodeling caused by a myocardial infarction (MI) is responsible for almost 70% of the 5 million cases of heart failure in the United States (Mozaffarian et al. 2016). Early infarct expansion or stretching has been associated with poor long-term prognosis (Eaton et al. 1979; Erlebacher et al. 1984; Weisman and Healy 1987) and has been identified as the mechanical phenomenon that initiates and sustains the process of adverse post-MI LV remodeling that leads to heart failure (Epstein et al. 2002; Jackson et al. 2003; Jackson et al. 2002; Kramer et al. 1993; Lima et al. 1985; Pilla et al. 2005). Infarct expansion causes abnormal stress distribution in myocardial regions within and outside the MI, especially in the adjacent normally perfused borderzone (BZ) region. With time, increased regional stress is the impetus for maladaptive biologic processes, such as matrix metalloproteinase activation, that inherently alter the contractile properties of normally perfused myocardium (Wilson et al. 2003). Once initiated, these maladaptive processes lead to a heart failure phenotype that is difficult to reverse by medical or surgical means.

We have demonstrated that externally affixed ventricular restraint early after MI reduces infarct expansion, moderates regional stress distribution, improves BZ contractile function and, most importantly, limits long-term global LV remodeling in large-animal MI models (Blom et al. 2007; Enomoto et al. 2005; Kelley et al. 1999; Moainie et al. 2002; Pilla et al. 2005). Although these studies have established the prevention of early infarct expansion as a potentially important therapeutic goal, it is unlikely that the surgical placement of restraining devices early after MI will gain widespread acceptance and application. As a result, we have done extensive experimental work to study the effect of injecting percutaneously deliverable biomaterials into the infarct to limit global LV remodeling (Ifkovits et al. 2010; Rodell et al. 2016; Ryan et al. 2009; Tous et al. 2011). While our results have demonstrated improvement in remodeling, the effect of these materials on regional myocardial stress distribution and BZ contractile function has not been fully established. In this study, we employed a state-of-the art MRI-based finite element (FE) model that employs subject-specific LV geometry to assess the effect of early post-MI infarct delivery of a novel shear-thinning biomaterial system on regional post-MI contractile function and regional myocardial stress distribution at 8 weeks after MI in an ovine infarct model.

Materials and Method

Infarct model

The data examined in the current study were collected in the course of a preceding study by Rodell et al (Rodell et al. 2016) wherein protocols complied with the University of Pennsylvania's Institutional Animal Care and Use Committee and animal care was in agreement with the National Institute of Health's guidelines for the care and use of

laboratory animals (NIH Publication 85-23, revised 1996). In brief, Dorset sheep (adult male, 45kg) underwent left thoracotomy to expose the heart. Posterolateral infarction was produced by suture ligation of obtuse marginal branches, selected on a case dependent basis to result in infarcts comprising approximately 20-25% of the left ventricle and involving the posterior papillary. A set of MRI-compatible platinum wire markers were sutured to the epicardium around the infarct boundary, identified by visible blanching of the infarcted tissue, immediately following infarction to enable infarct contouring from subsequent MRI acquisitions. Sixteen injections (0.3 mL each) of saline (MI control, n=6) or dual-crosslinking hydrogels (hydrogel treatment, n=6) were performed within the infarcted region 30 minutes post ligation. The injection pattern was a 4x4 grid, with the outermost injections placed approximately 1 cm away from the BZ. The dual-crosslinking (DC) hydrogels were prepared by separate modification of hyaluronic acid (HA) by both adamantane and thiols (Ad-HA-SH) or β-cyclodextrin and methacrylates (CD-MeHA), with injectable hydrogels formed by their combination at a pH of 5 under sterile conditions as previously reported (Rodell et al. 2016; Rodell et al. 2015).

Magnetic resonance (MR) imaging and analysis

At 8 weeks post-infarction, MR image acquisition was performed (3T MAGNETOM Trio; Siemens; Malvern, PA) under maintained anesthesia (1-2% isoflurane) with cardiac gating using LV placement of a pressure transducer (Millar Instruments; Houston, TX), with magnetic tagging triggered at onset of systole. Recorded pressures were later used to determine loading in the model. 3D SPAMM was performed to enable generation of animal-specific LV geometry and determination of corresponding tissue displacement fields (field of view = 260 mm × 260 mm, acquisition matrix = 256 × 128, pixel size = 1.015 mm × 1.015 mm, repetition time = 34.44 ms, tag spacing = 6 mm, bandwidth = 331 Hz/pixel, slice thickness = 2 mm, averages = 4) (Xu et al. 2010). Late-gadolinium enhanced (LGE) images were acquired 15 minutes following bolus administration of 0.1 mmol/kg gadobenate dimeglumine (MultiHance; Bracco Diagnostics; Cranbury, NJ) to confirm designation of the infarct region (field of view = 218 x 350 mm, acquisition matrix = 256 x 160, pixel size = 1.37x1.37 mm, repetition time = 5.50 ms, echo time = 2.42 ms, BW 244 Hz/pixel, slice thickness = 4 mm, averages = 2). The hydrogel distribution was examined following intramyocardial injection in vivo, explanation of the tissue, and hydrogel visualization by a T_2-weighted turbo spin echo pulse sequence (field of view = 100 x 80 mm, acquisition matrix = 320 x 256, pixel size = 0.3125 x 0. 3125 mm, repetition time = 1128 ms, echo time = 71 ms, slice thickness = 1 mm, averages = 4).

Both epicardial and endocardial contours of the LV were generated (ImageJ; Bethesda, MD) from 3D SPAMM images at the onset of systole to enable strain calculation by application of optical flow methods (Xu et al. 2010). Contours were similarly generated at early diastole to generate the animal-specific reference geometry for the FE model, including isolation of the endocardial and epicardial segments of the infarct region, which was aided by synchronization with LGE images. Endocardial contours were used to determine the end-systolic (ESV) and end-diastolic (EDV) LV volumes. The 3D distribution of hydrogel within the infarct was reconstructed using ITK-Snap (Yushkevich et al. 2006).

Finite Element modeling

Finite element models were created based on each animal-specific LV geometry at early diastole. This configuration was chosen because the stress in the LV is at a minimum. The geometry of LV wall was based on experimental measurements from MRI. The infarct region was defined based on the combination of LGE imaging and the MRI-compatible markers discussed previously. The BZ region was approximated as a 20-degree sector which transitions from the infarct region to the remote region, based on previous studies of 8 week posterolateral MI (Pilla et al. 2005; Pilla et al. 2015) (Figure 1).

Each animal-specific LV FE mesh (MI control, n=6; hydrogel treatment, n=6) was produced using tri-linear hexahedral brick elements, which were fit to 3D geometric surfaces that were generated from the endocardial and epicardial contours (TrueGrid; XYZ Scientific, Inc., Livermore, CA). The myofiber orientation in the remote, BZ, and infarct regions were assigned from epicardium to endocardium using the angles of −27 degrees to 88 degrees (Dorsey et al. 2015), −20 degree to 70 degree (Wu et al. 2009), and −5 degree to 26 degree (Dorsey et al. 2015) respectively. For the hydrogel treated group, the infarct region was modified to include a pattern of hydrogel injections embedded within the wall (Figure 2(b)). The pattern and volume were approximated from MR images of a representative in-vivo injection (Figure 2(a)). It should be noted that the MRI reconstruction, shown in Figure 2(a), was only conducted on a single animal. Therefore, the injection pattern in each of the six hydrogel treated models was approximated from this distribution. Since each injection was 0.3 ml, the total amount of volume added to the infarct region was 4.8 ml. The endocardial wall of each MI control and hydrogel treated LV model was loaded with a pressure boundary condition, based on the experimentally measured values from the pressure transducer. Boundary conditions were implemented at the base of the LV to fully constrain displacement on the epicardial-basal edge, while allowing the remaining basal nodes to move in the circumferential-radial plane.

Material response

The material response of the passive myocardium was represented using a nearly incompressible, transversely isotopic, hyperelastic constitutive law, which was defined using the following strain energy function (Guccione et al. 1991):

$$W_{myocardium} = \frac{C}{2}\left(e^{b_f E_{ff}^2 + b_t\left(E_{ss}^2 + E_{nn}^2 + E_{ns}^2 + E_{sn}^2\right) + b_{fs}\left(E_{fs}^2 + E_{sf}^2 + E_{fn}^2 + E_{nf}^2\right)} - 1\right) + \frac{\kappa}{2}(J-1)^2 \quad (1)$$

where E_{ij} are the deviatoric components of the Green-Lagrange strain tensor relative to the myofiber coordinate system (f = fiber direction, s = cross-fiber in-plane direction, n = transverse-fiber direction) and J is the determinant of the deformation gradient. The diastolic animal-specific material parameters, C in the remote region and C_I in the infarct region were optimized to match the corresponding EDV from MRI in each animal. Based on a previous study, the passive material parameters in the exponential function were assigned differently in the remote region (b_f, b_t, b_{fs}) and the infarct region (b_f_I, b_t_I, b_{fs}_I) for the MI control models and hydrogel treated models (MI: $b_f = 37.67$, $b_t = 17.39$, $b_{fs} = 23.12$,

$b_f\_I = 22.67$, $b_t\_I = 19$, $b_{fs}\_I = 18.12$; hydrogel: $b_f = 22.84$, $b_t = 3.46$, $b_{fs} = 12$, $b_f\_I = 15.28$, $b_t\_I = 8.32$, $b_{fs}\_I = 25.27$) (Dorsey et al. 2015). Note that the passive material parameters chosen in the BZ region were the same as the remote region at 8 weeks post-infarction, which is an assumption based on previous studies (Lee et al. 2011; Wenk et al. 2011). The bulk modulus was assigned as $\kappa = 1.0\,\text{GPa}$.

The material response of the hydrogel injections was represented using a nearly incompressible, isotopic, hyperelastic constitutive law, which was defined using the following strain energy function:

$$W_{injection} = \frac{E}{2(1+\nu)}\,\text{tr}(\mathbf{E}^2) + \frac{E}{6(1-2\nu)}\ln(J)^2 \tag{2}$$

where **E** is the deviatoric Green-Lagrange strain tensor, tr( ) is the trace operator, and ln( ) is the natural log operator. The material parameters for Young's modulus (E) were assigned based on the experimental measurements of the DC hydrogels at 8 weeks (E=4.5 kPa, determined in previous study (Rodell et al. 2016)), while the Poisson ratio (ν) was assigned a value of 0.499 (due to near incompressibility).

Systolic stress was modeled as the sum of the passive stress derived from the strain energy function and an active fiber directional stress component $\mathbf{T}_0$ (Guccione et al. 1993; Wenk et al. 2009), which was defined by a function of time, t peak intracellular calcium contraction, Ca_0, sarcomere length, l, and maximum isometric tension achieved at the longest sarcomere length T_{max}:

$$\mathbf{S} = pJ\mathbf{C}^{-1} + 2J^{-\frac{2}{3}}Dev\left(\frac{\partial\widetilde{W}}{\partial\widetilde{C}}\right) + \mathbf{T}_0\{t, Ca_0, l, T_{max}\} \tag{3}$$

where $Dev(\,)$ is the deviatoric operator and **C** is the right Cauchy-Green deformation tensor. At end-systole, the active fiber directional stress is defined as:

$$\mathbf{T}_0 = T_{max}\frac{Ca_0^2}{Ca_0^2 + \frac{(Ca_0)_{max}^2}{exp\left[B\left(I_R\sqrt{2E_{ff}+1} - l_0\right)\right] - 1}} \tag{4}$$

where B is a constant, $(Ca_0)_{max}$ is maximum peak intracellular calcium concentration, l_0 is the sarcomere length at which no active tension develops, and l_R is the reference sarcomere length in an un-loaded state. The material constants for active contraction were taken to be (Guccione et al. 1993): $Ca_0 = 4.35\ \mu\text{mol / L}$, $(Ca_0)_{max} = 4.35\ \mu\text{mol / L}$, $B = 4.75\ \mu\text{m}^{-1}$, $l_0 = 1.58\ \mu\text{m}$, and $l_R = 1.85\ \mu\text{m}$. It should be noted that these parameters were used in both the remote and BZ regions of the FE models. This assumption was based previous FE studies (Walker et al. 2005; Wenk et al. 2011) and on experiments performed by Shimkunas et al. (Shimkunas et al. 2014), which showed that there is no significant difference in the calcium sensitivity between remote and BZ tissue.

The systolic material parameter associated with the maximum isometric tension (T_{max}) was calculated in the remote and BZ regions using numerical optimization. In particular, the T_{max}

parameter within the remote region was designated as T_{max_R} and was assumed to be uniform throughout. Based on previous experimental and numerical studies of BZ contractility (Lee et al. 2011; Shimkunas et al. 2014), the T_{max} parameter was allowed to vary across the BZ region. Specifically, the contraction in the middle of the BZ ($T_{max\_mid\_B}$) and the contraction at the edge of the BZ ($T_{max\_edge\_B}$), which is located directly next to the infarct, were allowed to vary separately. These locations are shown schematically in Figure 1. The contraction parameter in the infarct region (T_{max_I}) was assigned to be zero, which was confirmed in previous work (Wenk et al. 2011). The initial search range in the optimization was set between 50 kPa and 400 kPa for T_{max_R} and between 10 kPa and 300 kPa for $T_{max\_mid\_B}$ and $T_{max\_edge\_B}$, while $T_{max\_I} = 0$ cross-fiber in-plane stress component equivalent to 40% of the fiber component was added based on previous studies of LV contraction (Walker et al. 2005).

Optimization

Each FE simulation was conducted in two phases, where the first phase represented passive diastolic filling and the second phase represented active systolic contraction to end-systole (LS-DYNA, Livermore Software Technology Corporation, Livermore, CA). The genetic algorithm (GA) was used to minimize the objective function, which was taken to be the sum of the squared error (SE) between the experimentally measured systolic data from MRI and FE predicted results, and was defined as

$$SE = \sum_{n=1}^{N} \sum_{i,j=1,2,3} w_n \left(E_{ij,n} - \bar{E}_{ij,n}\right)^2 + \left(\frac{V - \bar{V}}{\bar{V}}\right)^2 \quad (5)$$

where n is the location of a specific strain point within the myocardium, N is the total number of strain points, $E_{ij,n}$ and V are the FE predicted end-systolic strain and LV cavity volume, respectively. The over bar variables represent in-vivo measured values. Since there were fewer strain points measured in the BZ region compared to the remote region, the weight factor (w_n) for the SE in the BZ was set to 3 while the rest were set to 1. Additional details related to the parameters used in the GA are given in (Mojsejenko et al. 2015).

Statistical analysis

Data is presented as mean ± standard error (SEM) of the mean. For T_{max}, ES principal strain, and ES fiber stress, comparison between groups (MI control, hydrogel treated) was performed by two-tailed student's t-test with significant determined at $p < 0.05$. For the MI model and hydrogel model, statistical significance in different regions was determined by one-way ANOVA. Bonferroni test was used to account for multiple comparisons procedures with α=0.05.

Results

Estimation of Mechanical Properties

The average animal-specific diastolic material parameters, C in the remote region and C_I in the infarct region, were determined such that the model EDV matched the corresponding EDV from MRI. The values were found to be $C = 0.15 \pm 0.10$ kPa and $C\_I = 9.5 \pm 4.5$ kPa

for the MI control group, and $C = 0.89 \pm 0.24$ kPa and $C\_I = 23.7 \pm 4.6$ kPa for the hydrogel group, respectively. In order to further investigate the effects of the hydrogel on passive stiffness, the biaxial stress-strain relations were derived from the strain-energy function in Eqn (1) and then evaluated using the parameters from the remote and infarct regions, for both the treated and untreated groups. The modulus along the fiber direction was then estimated over the strain range of 0 to 0.05, using the tangent to the fiber direction stress-strain curve, similar to the approach taken in Dorsey et al. (Dorsey et al. 2015). It was found that the fiber direction modulus of the remote region (for both the treated and untreated groups) was approximately 42 ± 11 kPa. The fiber direction modulus for the infarct region in the MI control group was approximately 298 ± 93 kPa, while the hydrogel treated group was 620 ± 117 kPa. This implies that the treated infarct region is more than twice as stiff as the untreated infarct at 8 weeks post-MI, and it nearly 15 times stiffer than the remote myocardium.

The contractility parameter $T_{\max}$ was determined from optimization of all animal-specific models (Figure 3). For the MI control group, the parameter $T_{\max\_R} = 199.2 \pm 31.6$ kPa, $T_{\max\_mid\_B} = 79.7 \pm 12.7$ kPa, and $T_{\max\_edge\_B} = 21.5 \pm 5.3$ kPa. Relative to the remote region, this represents a 60% and 89% reduction in contractile force in the mid-BZ and edge-BZ regions of the untreated MI controls, respectively. For the hydrogel treated group, the parameter $T_{\max\_R} = 158.0 \pm 25.4$ kPa, $T_{\max\_mid\_B} = 129.8 \pm 17.4$ kPa, and $T_{\max\_edge\_B} = 112.3 \pm 17.1$ kPa. Relative to the remote region, this represents only an 18% and 29% reduction in contractile force in the mid-BZ and edge-BZ regions of the hydrogel treated animals, respectively.

In the remote region, the difference in contractile function between the treated and untreated animals was not associated with any statistical significance (p=0.334) (Figure 3). In contrast, the contractility in the mid-BZ and edge-BZ regions predicted in the hydrogel treated group were higher and significantly different from the MI control group (p*=0.042 and p*<0.001, respectively) (Figure 3). Additionally, within the MI control group the contractile function was significantly different when comparing the remote region to the mid-BZ and edge-BZ regions (p*=0.001 and p*<0.001, respectively) (Figure 3). However, the tissue contractile function within the hydrogel treated group was similar when comparing between the remote region and BZ regions, i.e., no statistical significance (p=0.308) (Figure 3). These results indicate that the BZ tissue in a treated animal has higher contractility compared to an untreated animal.

In terms of the fit achieved during the optimization, the average SE value for the MI control group was 25.1 ± 2.1 and for the hydrogel treated group was 21.9 ± 2.9. After decreasing monotonically during each optimization, the value of the objective function remained unchanged during the last five successive iterations. At that stage, it was assumed that the parameter values had converged to a unique solution within the designated parameter space. As an additional verification test, the search ranges for all of the parameters were varied by ± 25%. It was found that the final results were virtually unaffected. It is worth noting that the optimizations were also conducted with a uniform value of $T_{\max}$ in the BZ, which actually led to a worse fit between the MRI data and FE model predictions. Specifically, allowing BZ

contractility to vary spatially resulted in SE values that were improved by 3% and 4% for the MI control group and hydrogel treated group, respectively.

Systolic Principal Strains

In order to further explore the effects of hydrogel treatment on BZ function, the minimum principal strain (which relates to systolic shortening) and the maximum principal strain (which relates to radial thickening) were assessed at ES. In the BZ region, the minimum principal strain (ε_{min}) of the hydrogel group was higher and significantly different from the MI control group (p*=0.007) (Figure 4a). Additionally, in the MI control group, ε_{min} was significantly decreased in the BZ region compared to the remote region (p**=0.003) (Figure 4a). It should be noted that ε_{min} in the hydrogel group was similar when comparing between the remote region and BZ region, i.e., there is no statistically significant difference in shortening (p=0.086) (Figure 4a).

With respect to the maximum principal strain (ε_{max}), in the BZ region ε_{max} of the hydrogel group was higher and significantly different from the MI control group (p*=0.036) (Figure 4b). Additionally, in the MI control group, ε_{max} was significantly decreased in the BZ region compared to the remote region (p**=0.049) (Figure 4b). Similar to ε_{min}, the value of ε_{max} in the hydrogel group was similar when comparing between the remote region and BZ region, i.e., there is no statistically significant difference in thickening (p=0.642) (Figure 4b).

LV Wall Geometry

The average wall thickness within the infarct region at end-diastole for the MI control group and hydrogel treated group were 0.5±0.02 cm and 1.05±0.06 cm, respectively. In the BZ region, the average wall thickness was measured to be 0.64±0.01 cm and 0.86±0.04 cm for MI and hydrogel groups, respectively. In the remote region, the average wall thickness in the MI group was 0.98±0.05 cm while in the hydrogel group was 0.99±0.05 cm. This indicates that the DC hydrogel treatment reduced wall thinning at 8 weeks post-infarction and a significant difference was observed between the two groups (Rodell et al. 2016). It should be noted that additional data related to the LV cavity volumes, ejection fraction, and infarct area, for both the control and treated groups, have been previously reported (Rodell et al. 2016).

Regional Stress Distribution

The regional ES fiber stress distribution is given in Table 1. The average ES fiber stress in the infarct region of the hydrogel treated group was significantly reduced by 40% relative to the MI control group (p*=0.025). The average ES fiber stress of the hydrogel treated group in the BZ region was also significantly reduced by 35% relative to the MI control group (p*=0.003). In the remote region, the ES fiber stress showed a significant reduction of 34% compared to the MI control group (p*=0.014). The end-systolic fiber stress distribution in different regions of the mid-ventricle wall are shown for a representative hydrogel injection case (Figure 5a) and a representative MI control case (Figure 5c). Figures 5b and 5d define the different material regions for evaluating the fiber stress distribution, and also show the differences in wall thickness at end-systole.

Discussion

Despite the established efficacy and widespread availability of reperfusion therapy, myocardial infarction resulting from coronary artery disease and subsequent adverse LV remodeling remains a leading cause of heart failure (Mozaffarian et al. 2016). In the majority of acute MI patients, the LV function is initially preserved and only after months or years do symptoms of heart failure develop. The severity of the LV response to MI (i.e. LV remodeling) is determined by the size, location and transmurality of the infarct. We have previously shown that the dysfunctional BZ becomes more hypocontractile and progresses to involve additional perfused myocardium as remodeling continues and heart failure develops (Jackson et al. 2002).

Considering that external restraint devices, in the form of mesh jackets and patches, are not likely to achieve widespread clinical application because of the invasive surgical procedures that would be required in the early post-MI period to place them, our group and others have begun to explore and develop the use of hydrogel biomaterials to modify infarct material characteristics to limit or prevent progressive infarct expansion (Ifkovits et al. 2010; Rodell et al. 2016; Ryan et al. 2009; Tous et al. 2011). The use of such materials holds the potential for percutaneous, catheter-based approaches for beneficially altering the post-MI LV remodeling process. In recent years, a number of experimental and computational studies have investigated the capacity for injectable hydrogels to assuage LV remodeling through mechanical stabilization of the MI region. These studies have been expertly reviewed (Zhu et al. 2017) and highlight the need for hydrogels of appropriate stiffness, which may be easily delivered in a clinical setting. The novel shear-thinning biomaterial system tested in this study is an emerging candidate for translation into patients because it can be administered through long, narrow catheters but at the same time can be engineered to the appropriate stiffness for optimally limiting infarct expansion (Rodell et al. 2015).

Utilizing our state-of-the art MRI-based FE modeling approach, it was found that contractility in the BZ of animals treated with hydrogel injection was significantly higher than untreated controls, indicating that function is better retained due to treatment (Figure 3). In both the MI control and hydrogel groups, the variation of contractility across the BZ was very close to linear, which is in good agreement with previous experimental and numerical studies of sheep with MI (Lee et al. 2011; Shimkunas et al. 2014). The contractility results were reinforced by the fact that the magnitude of ES principal strain in the BZ region of the hydrogel treated group was significantly higher when compared to the MI control group (Figure 4). Additionally, the strain in the BZ region of the hydrogel treated group was similar to the remote region, which again implies the preservation of function. This result shows strong agreement with purely MRI-based studies, which found that ES principal strains were higher in animals treated with hydroxyapatite-based biomaterial injections (implying stronger contraction) (McGarvey et al. 2015). It was also found that the passive stiffness of the treated infarct region was greater than the untreated control. Additionally, the wall thickness in the infarct and BZ regions were significantly higher in the treated animals. Both of these factors are likely contributors to the fact that end-systolic fiber stress was greatly reduced in the BZ of treated animals.

There are several limitations in the current study. The hydrogel distribution was only imaged in a single animal. However, it should be noted that examination of the hydrogel distribution could not be conducted in all animals, since this would require the animal be sacrificed after injection to image gel distribution by MRI of the explanted tissue. The example shown (Figure 2) is assumed to be representative of the distribution in other animals, since the same injection pattern was used in every animal. The pericardium was not included in the LV models. This will be incorporated in future studies. Finally, it was assumed that the passive stiffness in the BZ region was the same as that in the remote region. This assumption will be explored further in future studies.

In conclusion, treatment with hydrogel injection significantly improved BZ function and reduced LV remodeling, via altered MI properties. These changes are linked to a reduction in the ES fiber stress experienced in the BZ myocardium surrounding the infarct. The current results, in conjunction with those reported previously, imply that the novel shear-thinning hydrogel system used in this study should be a viable therapy for mitigating adverse LV remodeling after MI.

Acknowledgements

This study was supported by a Predoctoral Fellowship from the American Heart Association (C. Rodell), by National Institutes of Health grants R01 HL063954 (R. Gorman) and R01 HL111090 (J. Burdick), by a grant from the National Science Foundation CMMI-1538754 (J. Wenk), and by a grant from the Shandong Province Natural Science Foundation, China ZR201709220101 (H. Wang).

References

Blom AS et al. (2007) Ventricular restraint prevents infarct expansion and improves borderzone function after myocardial infarction: a study using magnetic resonance imaging, three-dimensional surface modeling, and myocardial tagging Ann Thorac Surg 84:2004–2010 doi:10.1016/j.athoracsur.2007.06.062 [PubMed: 18036925]

Dorsey SM et al. (2015) MRI evaluation of injectable hyaluronic acid-based hydrogel therapy to limit ventricular remodeling after myocardial infarction Biomaterials 69:65–75 [PubMed: 26280951]

Eaton LW, Weiss JL, Bulkley BH, Garrison JB, Weisfeldt ML (1979) Regional cardiac dilatation after acute myocardial infarction: recognition by two-dimensional echocardiography N Engl J Med 300:57–62 doi:10.1056/NEJM197901113000202 [PubMed: 758578]

Enomoto Y et al. (2005) Early ventricular restraint after myocardial infarction: extent of the wrap determines the outcome of remodeling Ann Thorac Surg 79:881–887; discussion 881-887 doi:10.1016/j.athoracsur.2004.05.072 [PubMed: 15734399]

Epstein FH, Yang Z, Gilson WD, Berr SS, Kramer CM, French BA (2002) MR tagging early after myocardial infarction in mice demonstrates contractile dysfunction in adjacent and remote regions Magn Reson Med 48:399–403 doi:10.1002/mrm.10210 [PubMed: 12210951]

Erlebacher JA, Weiss JL, Weisfeldt ML, Bulkley BH (1984) Early dilation of the infarcted segment in acute transmural myocardial infarction: role of infarct expansion in acute left ventricular enlargement J Am Coll Cardiol 4:201–208 [PubMed: 6234343]

Guccione JM, McCulloch AD, Waldman LK (1991) Passive material properties of intact ventricular myocardium determined from a cylindrical model Journal of biomechanical engineering 113:42–55 [PubMed: 2020175]

Guccione JM, Waldman LK, McCulloch AD (1993) Mechanics of active contraction in cardiac muscle: Part II--Cylindrical models of the systolic left ventricle Journal of biomechanical engineering 115:82–90 [PubMed: 8445902]

Ifkovits JL et al. (2010) Injectable hydrogel properties influence infarct expansion and extent of postinfarction left ventricular remodeling in an ovine model Proc Natl Acad Sci U S A 107:11507–11512 doi:10.1073/pnas.1004097107 [PubMed: 20534527]

Jackson BM et al. (2003) Border zone geometry increases wall stress after myocardial infarction: contrast echocardiographic assessment American journal of physiology Heart and circulatory physiology 284:H475–479 doi:10.1152/ajpheart.00360.2002 [PubMed: 12414441]

Jackson BM et al. (2002) Extension of borderzone myocardium in postinfarction dilated cardiomyopathy J Am Coll Cardiol 40:1160–1167; discussion 1168–1171 [PubMed: 12354444]

Kelley ST et al. (1999) Restraining infarct expansion preserves left ventricular geometry and function after acute anteroapical infarction Circulation 99:135–142 [PubMed: 9884390]

Kramer CM et al. (1993) Regional differences in function within noninfarcted myocardium during left ventricular remodeling Circulation 88:1279–1288 [PubMed: 8353890]

Lee LC et al. (2011) A novel method for quantifying in-vivo regional left ventricular myocardial contractility in the border zone of a myocardial infarction Journal of biomechanical engineering 133:094506 doi:10.1115/1.4004995 [PubMed: 22010752]

Lima JA, Becker LC, Melin JA, Lima S, Kallman CA, Weisfeldt ML, Weiss JL (1985) Impaired thickening of nonischemic myocardium during acute regional ischemia in the dog Circulation 71:1048–1059 [PubMed: 3986975]

McGarvey JR et al. (2015) Injectable microsphere gel progressively improves global ventricular function, regional contractile strain, and mitral regurgitation after myocardial infarction Ann Thorac Surg 99:597–603 doi:10.1016/j.athoracsur.2014.09.014 [PubMed: 25524397]

Moainie SL et al. (2002) Infarct restraint attenuates remodeling and reduces chronic ischemic mitral regurgitation after postero-lateral infarction Ann Thorac Surg 74:444–449; discussion 449 [PubMed: 12173827]

Mojsejenko D et al. (2015) Estimating passive mechanical properties in a myocardial infarction using MRI and finite element simulations Biomech Model Mechanobiol 14:633–647 doi:10.1007/s10237-014-0627-z [PubMed: 25315521]

Mozaffarian D et al. (2016) Heart Disease and Stroke Statistics-2016 Update: A Report From the American Heart Association Circulation 133:e38–360 doi:10.1161/CIR.0000000000000350 [PubMed: 26673558]

Pilla JJ et al. (2005) Early postinfarction ventricular restraint improves borderzone wall thickening dynamics during remodeling Ann Thorac Surg 80:2257–2262 doi:10.1016/j.athoracsur.2005.05.089 [PubMed: 16305885]

Pilla JJ, Koomalsingh KJ, McGarvey JR, Witschey WR, Dougherty L, Gorman JH, Gorman RC (2015) Regional myocardial three-dimensional principal strains during postinfarction remodeling The Annals of thoracic surgery 99:770–778 [PubMed: 25620591]

Rodell CB et al. (2016) Injectable shear-thinning hydrogels for minimally invasive delivery to infarcted myocardium to limit left ventricular remodeling Circulation: Cardiovascular Interventions 9:e004058 [PubMed: 27729419]

Rodell CB, MacArthur JW, Dorsey SM, Wade RJ, Wang LL, Woo YJ, Burdick JA (2015) Shear-Thinning Supramolecular Hydrogels with Secondary Autonomous Covalent Crosslinking to Modulate Viscoelastic Properties In Vivo Advanced Functional Materials 25:636–644 doi:10.1002/adfm.201403550 [PubMed: 26526097]

Ryan LP et al. (2009) Dermal filler injection: a novel approach for limiting infarct expansion Ann Thorac Surg 87:148–155 doi:10.1016/j.athoracsur.2008.09.028 [PubMed: 19101288]

Shimkunas R et al. (2014) Myofilament dysfunction contributes to impaired myocardial contraction in the infarct border zone American journal of physiology Heart and circulatory physiology 307:H1150–1158 doi:10.1152/ajpheart.00463.2014 [PubMed: 25128171]

Tous E et al. (2011) Influence of injectable hyaluronic acid hydrogel degradation behavior on infarction-induced ventricular remodeling Biomacromolecules 12:4127–4135 doi:10.1021/bm201198x [PubMed: 21967486]

Walker JC et al. (2005) MRI-based finite-element analysis of left ventricular aneurysm American journal of physiology Heart and circulatory physiology 289:H692–700 doi:10.1152/ajpheart.01226.2004 [PubMed: 15778283]

Weisman HF, Healy B (1987) Myocardial infarct expansion, infarct extension, and reinfarction: pathophysiologic concepts Prog Cardiovasc Dis 30:73–110 [PubMed: 2888158]

Wenk JF et al. (2011) Regional left ventricular myocardial contractility and stress in a finite element model of posterobasal myocardial infarction Journal of biomechanical engineering 133:044501 [PubMed: 21428685]

Wenk JF et al. (2009) A method for automatically optimizing medical devices for treating heart failure: designing polymeric injection patterns Journal of biomechanical engineering 131:121011 doi:10.1115/1.4000165 [PubMed: 20524734]

Wilson EM et al. (2003) Region- and type-specific induction of matrix metalloproteinases in post-myocardial infarction remodeling Circulation 107:2857–2863 doi:10.1161/01.CIR.0000068375.40887.FA [PubMed: 12771000]

Wu M-T et al. (2009) Sequential changes of myocardial microstructure in patients postmyocardial infarction by diffusion-tensor cardiac MR correlation with left ventricular structure and function Circulation: Cardiovascular Imaging 2:32–40 [PubMed: 19808562]

Xu C et al. (2010) Deformation analysis of 3D tagged cardiac images using an optical flow method Journal of Cardiovascular Magnetic Resonance 12:12–19 [PubMed: 20222980]

Yushkevich PA, Piven J, Hazlett HC, Smith RG, Ho S, Gee JC, Gerig G (2006) User-guided 3D active contour segmentation of anatomical structures: significantly improved efficiency and reliability Neuroimage 31:1116–1128 doi:10.1016/j.neuroimage.2006.01.015 [PubMed: 16545965]

Zhu Y, Matsumura Y, Wagner WR (2017) Ventricular wall biomaterial injection therapy after myocardial infarction: Advances in material design, mechanistic insight and early clinical experiences Biomaterials 129:37–53 doi:10.1016/j.biomaterials.2017.02.032 [PubMed: 28324864]

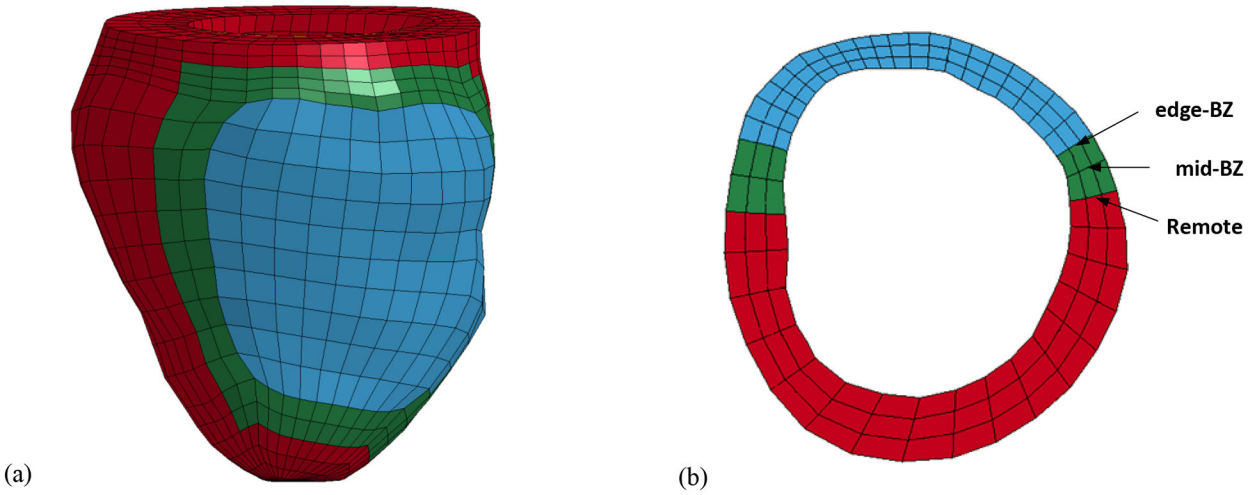

(a) (b)

Figure 1:

(a) Animal-specific FE model. The red elements represent the remote region, green elements are BZ region, and blue elements are the infarct region. (b) Short axis cross-section view of the animal-specific FE model near mid-ventricle.

(a)

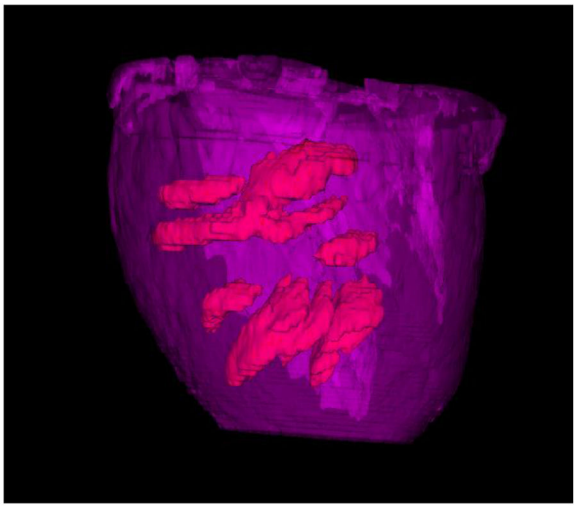

(b)

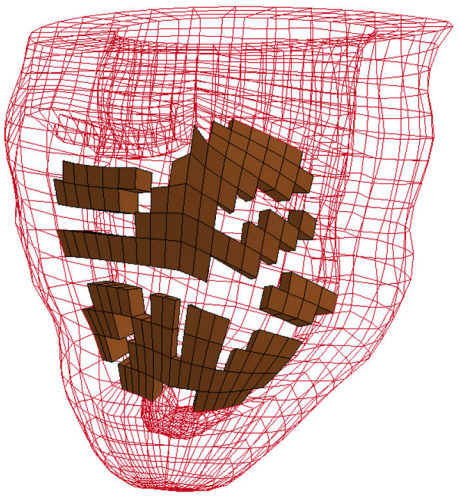

Figure 2:

(a) Image reconstruction from T_2-weighted MRI data of retained hydrogel (red) distributed within the infarct region (purple) in vivo. (b) Example of FE model with approximated hydrogel injection pattern (brown) within the infarct region.

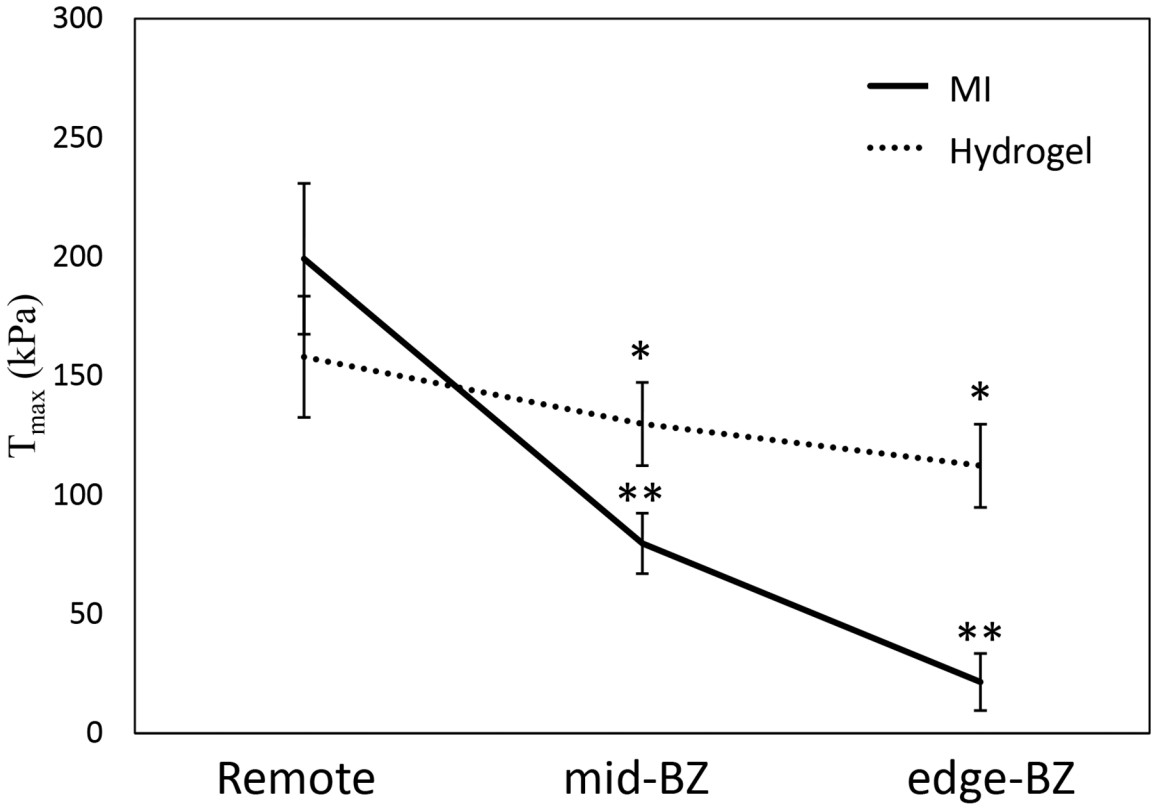

Figure 3:

Comparison of the T_{max} distribution between the MI control group and hydrogel treated group in the remote region and BZ region. (*p < 0.05 relative to MI control; **p < 0.05 relative to remote region)

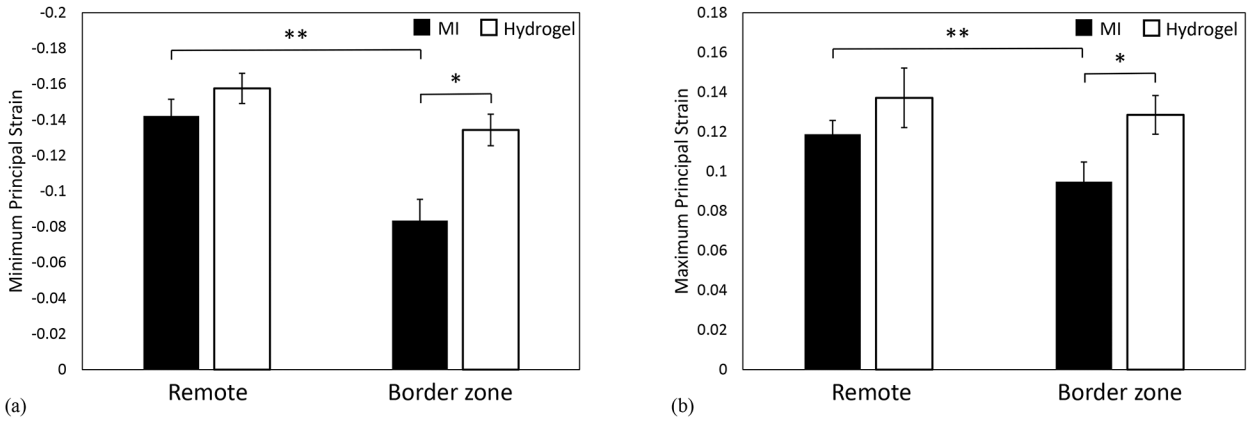

Figure 4:

(a) Comparison of the ES minimum principal strain between the MI control group and hydrogel treated group in the remote region and BZ region. (b) Comparison of the ES maximum principal strain between the MI control group and hydrogel treated group in the remote region and BZ region. (*$p < 0.05$ relative to MI control; **$p < 0.05$ relative to remote region)

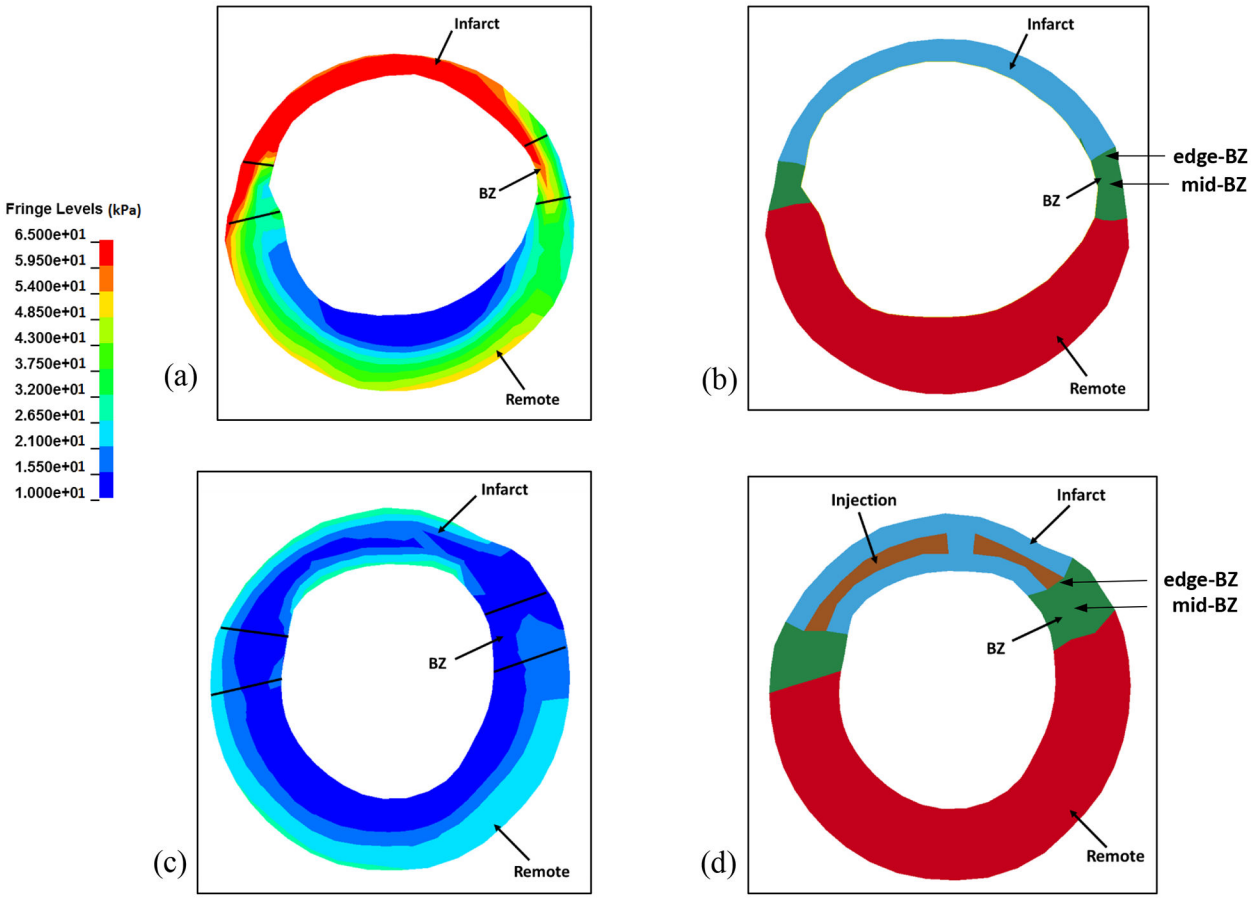

Figure 5:

(a) End-systolic fiber stress distribution in cross-section view of an animal-specific MI control FE model near mid-ventricle. (b) Cross-section view of the MI FE model at end-systole in same location. (c) End-systolic fiber stress distribution in cross-section view of an animal-specific hydrogel treated FE model near mid-ventricle. (d) Cross-section view in the hydrogel treated FE model at end-systole in same location.

Table 1:

Comparison of end-systolic fiber stress (kPa) between the MI control group and hydrogel treated group in the Remote, Border zone, and Infarct regions, respectively. *p < 0.05 compared to MI control.

	Remote	Border zone	Infarct
MI control	21.86±1.51	29.84±1.98	47.25±6.14
Hydrogel treated	14.12±2.31*	19.53±1.69*	28.49±3.78*